Oblique wave-wave interactions of nonlinear near-surface internal waves in the Strait of Georgia

C. Wang[1] and R. Pawlowicz[2]

Received 7 March 2012; revised 11 May 2012; accepted 18 May 2012; published 30 June 2012.

[1] Although nonlinear interactions that occur when two large internal waves collide at oblique angles are often observed in the natural world, quantitative and theoretical aspects of these interactions are only poorly understood. The available analyses are generally theoretical or the result of limited numerical experimentation, with few (if any) quantitative field measurements. Here we describe four cases of internal wave interactions, two of which involve the fundamentally non-steady generation of "Mach stems" at the site of the interaction, observed in the Strait of Georgia, Canada. Details of the interactions are quantified using time sequences of photogrammetrically rectified oblique images obtained from a circling aircraft, while simultaneous observations are made of water column properties from a surface vessel. The imaging technique allows us to estimate the speed and direction of each wave, as well as details of phase shifts induced by interactions. An existing small-amplitude theory is applied but is found to overestimate the likelihood of Mach interactions at large amplitude.

Citation: Wang, C., and R. Pawlowicz (2012), Oblique wave-wave interactions of nonlinear near-surface internal waves in the Strait of Georgia, *J. Geophys. Res.*, *117*, C06031, doi:10.1029/2012JC008022.

1. Introduction

[2] What happens when waves in two spatial dimensions, moving in different directions, cross each other? When wave amplitudes are small, then the dynamics are "linear" and the waves do not interact. They pass through each other without changing their amplitude, wavelength, or propagation direction. However, when wave amplitudes are large, which can be defined in a mathematically precise way, then their speed can depend to some extent on the wave amplitude, with larger waves moving faster. When such waves cross, amplitudes superimpose, and one might expect a region with an even larger displacement at the intersection. What are the consequences of this larger displacement? Larger displacement implies larger currents. In some cases larger displacement can lead to breaking and hence enhanced mixing. In others, there may be a resonant transfer of energy between different waves. Or will waves still pass through each other without change? All of these factors may be important in determining the propagation and dissipation of internal wave energy, and the effects of internal waves on ocean structures such as oil platforms.

[3] This problem is both obscure and almost completely unstudied, yet widespread and ever-present in the natural world. Although there is a vast literature on non-linear wave propagation, and entire books and even fields of mathematics [e.g., *Osborne*, 2010] devoted to such interactions when both waves are proceeding in the same direction the useful literature associated with the oblique interaction of nonlinear waves consists of about a dozen papers over the past 35 years. On the other hand, these interactions are easily seen in surface waves on flat beaches. They can also be identified to some degree or other in almost any satellite image containing a number of internal wave "packets". This is because, under certain conditions, the velocity field associated with internal waves can modulate the surface wavefield, creating "slicks" above the wave crests. Changes in surface roughness associated with these slicks are highly visible.

[4] However, quantitative analysis using satellite images is difficult because they provide only "snapshots" of the wave at widely-spaced times. Only qualitative information can be derived about individual waves. Measurements from ships using either acoustic or lowered instruments very often can only provide data at a single point. Some studies have used collections of moored instruments, but it is hard to determine what occurs between moorings. In addition, changes along the wave crest from one part of the wave to another are not easy to see, and hence wave-wave interactions occurring when the two waves are propagating in different directions impossible to observe accurately. Due to the limitations of such observational methods, there are no geophysical observations known to us that quantitatively describe oblique interactions of individual internal waves.

[5] The purpose of this paper is then to describe what is known about oblique nonlinear wave interactions, and to use a novel observational technique involving time series of

[1]Physical Oceanography Laboratory, Ocean University of China, Qingdao, China.
[2]Department of Earth and Ocean Sciences, University of British Columbia, Vancouver, British Columbia, Canada.

Corresponding author: C. Wang, Physical Oceanography Laboratory, Ocean University of China, 238 Songling Rd., Qingdao, China, 266100. (cxwang@ouc.edu.cn)

0148-0227/12/2012JC008022

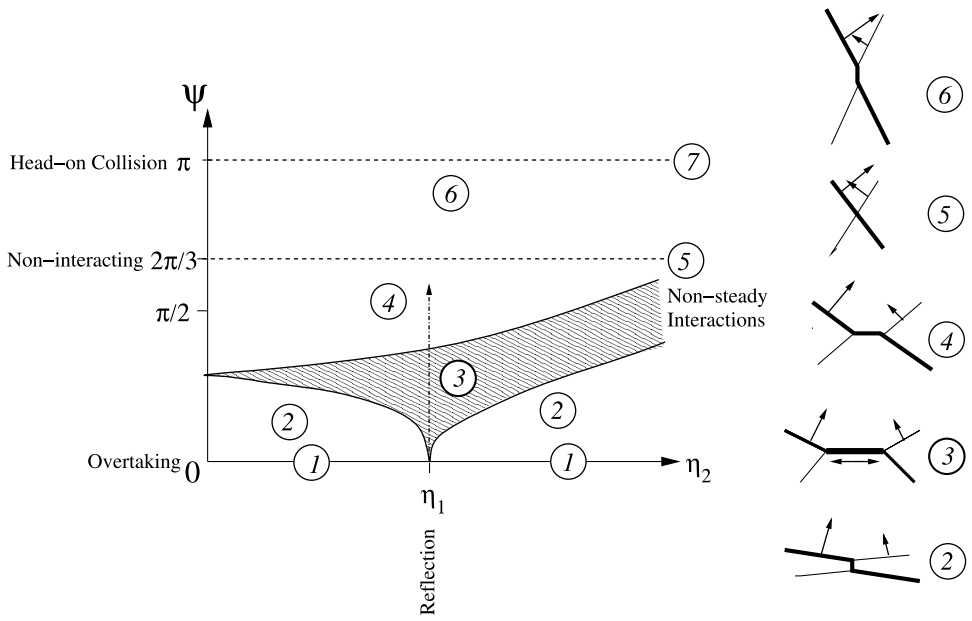

Figure 1. Schematic illustration of the types of interactions that can occur between two obliquely crossing solitons. At left is shown the regions for different interactions in a (η_2, ψ) parameter space. Cases are (1) overtaking, (2) obliquely overtaking, (3) non-steady Mach interaction, (4) regular interaction, (5) non-interacting at $\psi = 2\pi/3$, (6) obliquely colliding, (7) head-on colliding. Cases (1) and (2) are strong interactions and phase-conserving. Cases (3) and (4) are strong interactions and non-phase-conserving. Cases (6) and (7) are weak interactions and non-phase-conserving. Reflection cases occur when $\eta_1 = \eta_2$. At right are shown schematic overhead views of the interaction region between two different wave crests. Crests are shown as lines, with larger amplitudes appearing as thicker lines. Arrows show phase propagation speed and direction.

photogrammetrically rectified oblique aerial photos to characterize examples of oblique interactions between internal waves found in the natural world. The observational technique used is capable of determining both the speed and direction of individual waves, and this is supplemented by water column data about wave structure and ambient stratification [*Wang and Pawlowicz*, 2011]. It can also determine the degree to which an interaction is steady or non-steady.

[6] In the next section, oblique nonlinear wave interactions are classified and described on a theoretical basis. Theory is most advanced for shallow-water surface waves, but applications to internal waves are discussed. Then, the observational technique used to obtain data from internal waves in the Strait of Georgia, British Columbia, is briefly described. A number of interaction patterns are analyzed, and their characteristics compared with theory.

2. Theoretical Background

[7] Consider the interaction of two crossing waves, whose wave crests are straight and long enough that "edge" effects will not be important at the location of their crossing point. There is a certain difficulty here in reconciling this picture with time-dependent variations at the interaction location but some rationalization by recourse to reflection symmetries is possible when waves initially traveling parallel to a wall encounter a change in wall direction [e.g., *Melville*, 1980].

[8] Normalized wave amplitudes before any interaction are η_1 and η_2, which may be the same or different. Normalization is done by water depth for long surface waves, or by an effective depth for long internal waves in a stratified system. In the case of internal waves in a shallow stratified layer above an infinitely deep lower layer, then the effective depth is approximately the depth of the shallow layer.

[9] The angle between the wave normals $\bar{k}_{1,2}$ is called the interaction angle ψ, measured in radians. The location of each wave at time t is described by a phase $\theta_i = \bar{k}_i \cdot (\bar{x} - \bar{c}_i t)$, where $\bar{k}_i$ sets the length scale in the direction of propagation and $\bar{c}_i$ is the phase speed in that direction. For solitons the wave displacement is the largest near $\theta \approx 0$ and goes to zero for $|\theta| \gg 1$.

[10] A careful study of the literature finds that wave interactions of finite but small amplitude waves under these conditions can be categorized into no less than seven types (Figure 1). Different cases have been investigated by different authors, with some overlap. The general tool for theoretical investigations involves asymptotic expansions around particular cases (e.g., head-on or parallel propagation, similar or wildly dissimilar amplitude ratios, etc.), so that derived formulas that quantitatively define transition points agree only to first order, and hence are not exactly consistent with one another as they overlap outside their region of strict validity.

2.1. Oblique Interaction of KdV Waves

[11] The first comprehensive investigation of such wave-wave interactions was that of *Miles* [1977] who investigated small-amplitude shallow-water interactions between solitons of the form $\mathrm{sech}^2(\theta)$ governed by the Korteweg-de Vries (KdV)

equation. *Miles* [1977] classified the interaction processes of solitary waves into "symmetric" and "asymmetric", "strong" and "weak", "phase-conserving" and "non-phase-conserving", "regular" and "Mach" interactions.

[12] The interaction processes of solitary waves were classified into "symmetric" interactions (i.e. reflections at a wall) and "asymmetric" interactions by comparing the wave amplitude difference and the interaction angle. If two waves interact and their amplitude difference is small compared to the (radian) interaction angle, i.e. $|\eta_2' - \eta_1'| < \psi^2$, then their interaction can be treated as reflection to first order with one of the two interacting waves regarded as the incident wave and the other one as its image. Otherwise, it is an asymmetric interaction.

[13] Wave interactions were categorized into "strong" and "weak" according to the length of the interaction time and the magnitude of the resulting phase shift. A strong interaction occurs when the two solitary waves propagate in almost the same direction, interact for a relatively long time and emerge with phase shifts of order $O(1)$. Mathematically, an interaction is strong when $\left(\frac{\psi}{2}\right)^2 = O(\eta_{1,2}')$. Overtaking is the special case of a strong interaction when the interacting waves are propagating in the same direction. Strong interactions are intrinsically nonlinear.

[14] A weak interaction corresponds to the interaction of solitary waves propagating in very different directions, so that the interaction time is relatively short. Phase shifts are of order $O(\eta_{1,2}')$. A head-on collision is one special case of a weak interaction when the propagation directions of the interacting waves are opposite. Weak interactions permit superposition of the individual solutions to a first order approximation.

[15] An interaction is phase-conserving if the sum of the phases of the incoming waves is equal to the sum of the phases of the outgoing waves. The phase shift is defined by *Miles* [1977] as δ such that a wave described by $\mathrm{sech}^2(\theta)$, is expressed as $\mathrm{sech}^2(\theta - \delta)$ after phase shift δ. A positive phase shift means the wave appears to jump forward. Phase conserving interactions then have one wave jumping forward and one wave jumping backward. Interactions are found to be phase-conserving if the difference in wave amplitudes ($|\eta_2' - \eta_1'|$) is greater than the square of interaction angle (ψ^2), but not conserved if $|\eta_2' - \eta_1'| < \psi^2$. Symmetric or reflection problems are not phase-conserving.

[16] When two waves come from exactly opposite directions (case 7 of Figure 1), the angle between the two wave normals is 180°, and the interaction is a head-on collision. Typically both of the interacting waves are shifted backwards, relative to the location they would appear in without the interaction occurring (i.e. they experience a negative phase shift), although they continue propagating in the original directions. The interaction does not conserve phase since the sum of the phase shifts is negative. It is also a weak interaction.

[17] When the interaction angle is between 120° and 180°, the two interacting waves also both shift backward (case 6 of Figure 1). This is qualitatively not very different from the head-on collision case, although the degree of phase shift decreases as the interaction angle decreases. These nearly head-on cases are also weak interactions that do not conserve phase.

[18] When the angle between the wave normals of the two interacting waves is 120° (case 5), the two interacting waves experience no phase shift at all [*Matsuno*, 1998; *Grimshaw and Zhu*, 1994]. This occurs irrespective of any differences in wave amplitudes.

[19] When the interaction angle is 0°, then an interaction can only occur if the wave amplitudes are different. This is fundamentally asymmetric. Consider a larger wave overtaking a smaller wave (case 1). These waves interact for relatively long time and the interaction is classified as strong interaction. After an overtaking interaction, the larger wave appears ahead of the smaller wave, and its phase is advanced relative to where it would have been without the small wave appearing. Conversely, the smaller wave in front later appears behind, and its phase has shifted backward, i.e. it appears to have not moved as far as it would have without the interaction occurring. This kind of interaction is phase-conserving, because mathematically the backward and forward shifts cancel in a sum [*Miles*, 1977]. This is the most well-studied case.

[20] If these two waves, moving in roughly but not exactly the same direction (case 2, i.e. with small interaction angle), have different amplitudes, then one can treat the interaction as approximately (or locally) the same as case 1. These interactions are strong interactions. Moving along the crests is roughly the same as moving forward or backward in time in the 1D (case 1) interaction, and phase is again conserved. Note that for the above discussed cases the direction of propagation of the two waves remains unchanged by their interaction.

[21] However, we now have the additional possibility of two waves with the same amplitude interacting (central region of case 3, Figure 1). This cannot be an overtaking case since the speed of each wave has the same magnitude. However, it can occur for any non-zero interaction angle. This could also be considered the symmetric interaction that occurs as a wave hits a wall at an oblique angle (i.e. a reflection; see Figure 2a), with one wave being the incident wave and the other a reflected wave [e.g., *Melville*, 1980]. In such cases a third wave appears near the wall. This third wave is often called a "Mach stem", but in fact a further subdivision of cases exists and we classify these cases as either "regular" or "Mach" interactions.

2.2. Mach and Regular Interactions

[22] For small but finite amplitudes, Mach interactions (case 3 of Figure 1) occur for an intermediate range of angles under the condition [*Miles*, 1977] that

$$\psi_- < \sin^2\frac{\psi}{2} < \psi_+ \tag{1}$$

where

$$\psi_\pm = \frac{3}{4}\left(\sqrt{\eta_1'} \pm \sqrt{\eta_2'}\right)^2. \tag{2}$$

[23] If the amplitude of one of the waves gets very large, then the range of interaction angles for which the non-steady behavior occurs also increases, but reaches a maximum of about 127° [*Johnson*, 1982] (right side of case 3 in Figure 1). In the limit as the amplitude of the waves becomes very

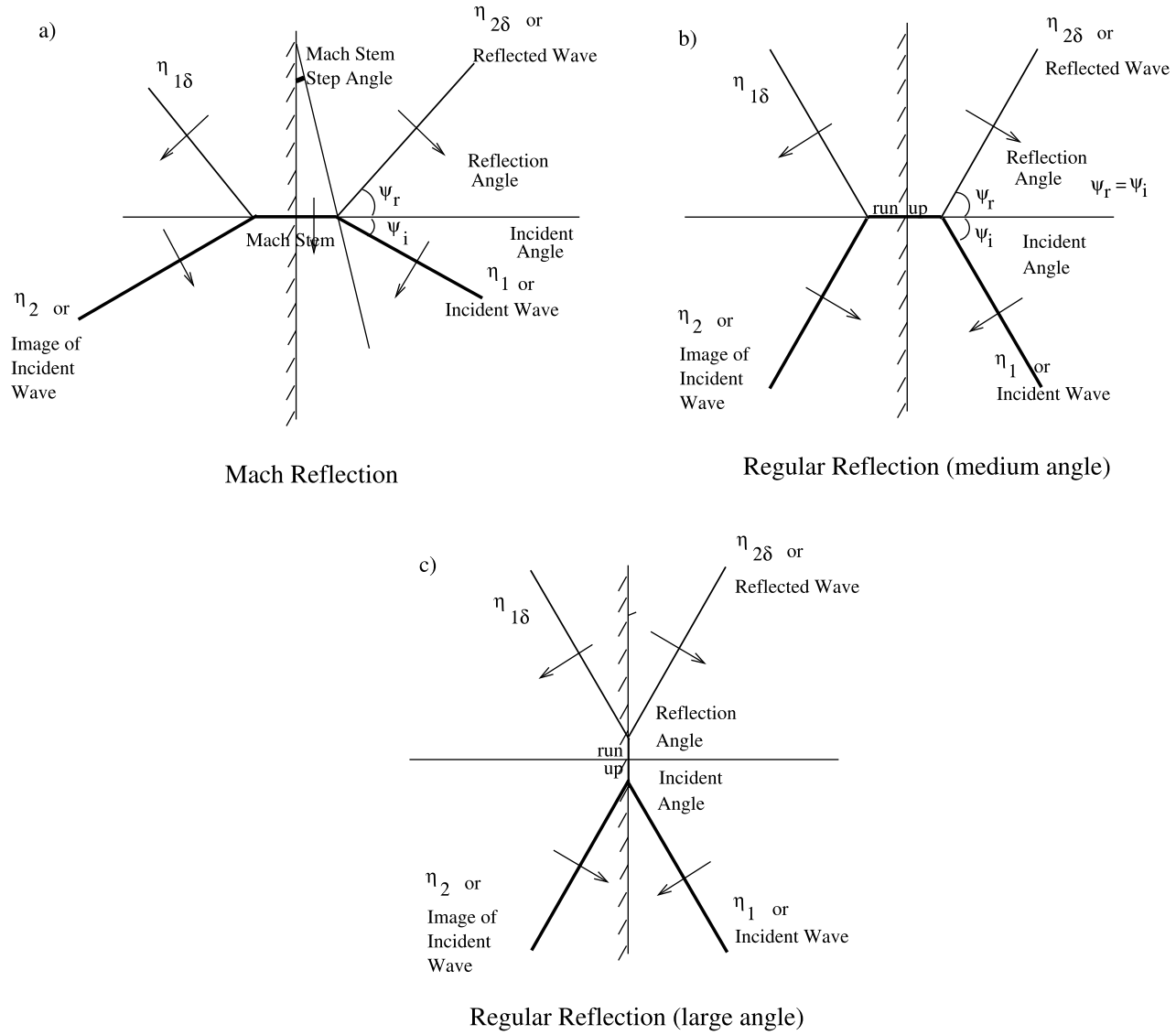

Figure 2. Schematic definition of Mach interaction and regular interaction of two waves η_1 and η_2, $(\eta_1, \eta_2) \rightarrow (\eta_{1\delta}, \eta_{2\delta})$. η_2 $(\eta_{1\delta})$ will be the image of η_1 $(\eta_{2\delta})$ for the reflection case. Figure 2a corresponds to case 3 of Figure 1. Figure 2b corresponds to case 4 of Figure 1. Figure 2c corresponds to case 6 of Figure 1. When incident waves are similar a plane of symmetry exists (hatched line),which can be replaced by a solid wall to create a reflection problem.

small, the range of angles for which Mach interactions occur also becomes small.

[24] For reflection problems where the two amplitudes are similar, Mach interactions occur for all angles up to a critical angle:

$$\psi < 2\sqrt{3\eta'_{1,2}} \tag{3}$$

[25] The name "Mach" arises because of its mathematical and geometrical similarity to shock-wave reflection problems in supersonic gas dynamics [*Whitham*, 1974]. In such interaction problems, in addition to the incoming and outgoing waves, a third wave appears, perpendicular to the wall. All three waves meet at a point away from the wall (Figure 2a). The length of the wave crest of this third wave (the "Mach stem") grows with time, and this implies that the propagation direction of the trailing wave will also change. The growth rate is given by a non-zero "step angle" ψ_*. The interaction is fundamentally non-steady.

[26] However, for interaction angles larger than the critical value (equation (1)) and less than 120° the stem no longer grows with time, appearing instead as a "bar" between two waves that are shifted forward by the interaction (case 4, not phase-conserving), but whose propagation directions are unchanged. The steady wave generated between the original waves and the phase shifted waves due to interaction is called runup (Figure 2b).

[27] More recently nonlinear wave interactions have been studied as a model for rogue waves [*Soomere and Engelbretcht*, 2006]. An overview of the practical application of certain properties of phase shifts, and the resulting

high wave hump during Mach interaction and nonlinear interaction of solitons can be found in *Soomere* [2007]. Although these kinds of interactions are sometimes also called Mach stems, and are also found as periodic solutions to the so-called Kadomtsev-Petviashvili equation [*Hammack et al.*, 1995], we shall label these as "regular" interactions and reserve the name "Mach stem" only for the fundamentally non-steady solutions.

[28] If we define $\varepsilon \equiv \frac{\psi}{2}/\sqrt{3\eta_i}$, then for reflection problems we have the following [*Tanaka*, 1993]:

[29] 1. $\varepsilon < 1$ for Mach reflection and $\varepsilon > 1$ for regular reflection.

[30] 2. Step angle $\psi_* = 0$ for regular reflection, but a nonzero $\psi_* = \sqrt{\eta_i'/3}(1-\epsilon)$ for Mach reflection, i.e. largest for shallowest angles.

[31] 3. The maximum runup at the wall is $\left(2 + \left(\frac{3}{2\sin^2\frac{\psi}{2}} - 3 + 2\sin^2\frac{\psi}{2}\right)\eta_i'\right)\eta_i$ for non-grazing regular reflection and the amplitude of Mach stem η_M is $(1+\varepsilon)^2\eta_i$ for Mach reflection. Thus the largest "stem" wave occurs at the transition between regular and Mach reflection, and is about four times the amplitude of the incident wave.

[32] 4. The amplitude of the reflected wave η_r equals the amplitude of the incident wave η_i for regular reflection but is only $\varepsilon^2\eta_i$ for Mach reflection. Thus at shallow angles the two waves may appear to merge with very little left of the original waves after they interact.

[33] 5. The angle of reflection ψ_r equals the angle of incidence ψ_i for regular reflection and $\sqrt{3\eta_i'}$ for Mach reflection.

[34] If the two amplitudes are only slightly different, with $|\eta_2' - \eta_1'| < \psi^2$ [*Miles*, 1977], so that the problem is approximately (or to first order only) a reflection problem, then one might expect a well-defined transition from case 2 behavior to case 3 behavior at some nonzero interaction angle, followed by a transition to case 4 behavior as the interaction angle increases.

2.3. Numerical and Laboratory Investigation

[35] After Miles' pioneering work, laboratory and numerical investigations were performed to test his theoretical results. *Melville* [1980] performed laboratory experiments. He supported Miles in predictions of critical angle, but the measured amplitude of the Mach stem at the wall in these experiments is considerably lower than predicted from Miles' theory. *Funakoshi* [1980, 1981] tested the theory using a numerical model. He stated that the discrepancy between Miles and Melville inthe amplitude of the Mach stem was due to the insufficient interaction time allowed in Melville's measurements.

[36] *Tanaka* [1993] also examined large amplitude wave interactions numerically. He concluded that Miles' results only apply to weakly nonlinear i.e. small amplitude wave cases with $\eta_{1,2}' \ll 1$. For larger amplitude waves, the effect of the large amplitude tends to prevent Mach reflection from occurring. If Mach reflection does take place for large amplitude waves, it will differ from small amplitude cases. The interaction will be "contaminated" by regular reflection with the amplitude of the reflected wave close to that of the incident wave. These results are closer to the analytical estimates of *Johnson* [1982]. Thus *Tanaka*'s [1993] conclusion was that Miles' results are apparently only quantitatively useful if the wave amplitudes are sufficiently small.

2.4. Internal Waves and Deep Water

[37] Although the above analysis was carried out for shallow water surface wave solitons, the equations used were of the KdV type and hence the results should be applicable to internal waves described by modes in a long-wave approximation as well. This is because the behavior of such modes may also be governed by KdV equations. However, one of the features of internal waves which distinguish them from surface waves is that there is an infinite set of modes and the interaction between different modes makes the interaction of internal waves more complicated than that of surface waves.

[38] Fortunately, according to *Liu and Hsu* [1998], almost all of the nonlinear internal waves observed in nature are Mode-1 depression waves. It is plausible (but unproven) that the interaction of internal solitary waves of the same mode can be treated like the surface solitary waves interactions [*Grimshaw and Zhu*, 1994]. The dependence of phase shift on the interaction angle and wave amplitudes is generally similar for both surface and internal waves, although slight differences have been reported in numerical studies [*Lynett and Liu*, 1998].

[39] In cases where a thin stratified layer appears above an infinitely deep lower layer, the internal waves are "long" only with respect to the depth of the stratified layer. These kinds of waves are described by the deep water Benjamin-Ono (BO) equation [*Benjamin*, 1966; *Ono*, 1975].

[40] Deep water solitons have novel characteristics compared to those in shallow water systems. For example, the BO solitons have a profile expressed in terms of algebraic functions, while KdV solutions are expressed by hyperbolic functions. The differing functions may suggest that the oblique interactions of shallow water waves and deep water waves differ fundamentally. However, according to *Grimshaw and Zhu* [1994], in either a shallow water (KdV) interaction or a deep water interaction, the only effect of interaction on the two interacting waves is a phase shift. Other investigations [*Matsuno*, 1998; *Oikawa*, 1984; *Grimshaw and Zhu*, 1994] have studied wave-wave interactions in deep water systems and although there are differences the general behavior is similar to KdV wave interactions. For head-on collisions of two BO solitons, it was shown analytically that the amplitudes of solitary waves did not change after interaction while both of the two waves were shifted backwards in phase. Also, at an interaction angle of 120°, both interacting waves in shallow water and deep water systems do not experience any phase shift. Therefore, the interactions between deep water solitary waves and between shallow water solitary waves have some resemblance.

[41] *Tsuji and Oikawa* [2001] numerically studied the oblique interactions of internal solitary waves in a deep two-layer fluid. Their wave amplitudes (nondimensionalized by the shallow layer depth) are as high as $\eta_i' = 3$. They found that Mach interaction did occur for small interaction angles ($\psi < 118°$). For interaction angles near $\psi = 106°$, maximum Mach stem amplitudes were generated. The critical angle is much smaller than that predicted using Miles' theory (misapplied at this large amplitude). The maximum Mach stem

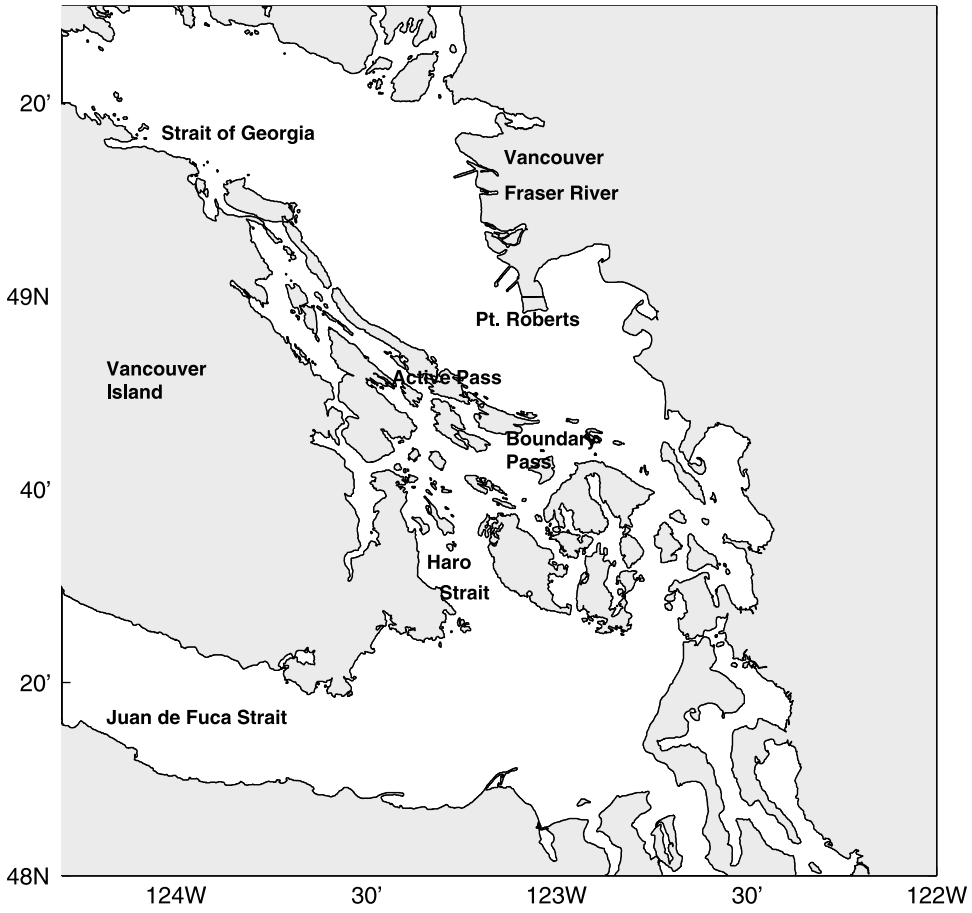

Figure 3. Map of the southern Strait of Georgia. The intensive field work for this paper research is carried out mostly in the region between Active Pass and Point Roberts.

amplitude exceeded the values for predicted shallow water waves.

[42] In summary, oblique interactions of solitons can be classified into a number of different categories. Of particular interest are the fundamentally unsteady Mach stem solutions, which occur for a restricted set of interaction angles and wave amplitudes. This is because Mach stems, involving the transfer of energy between different waves, evolve and can generate larger amplitude solitary waves. However, a very small number of experiments (mostly numerical) suggest that analytical formulas developed to describe the critical angles for Mach interactions (equation (1)) are not very accurate for waves of realistic amplitudes. In addition, it is only plausible (but not proven) that internal waves of a given mode can interact without losing energy to other modes, and that the oblique interactions of deep water solitons and shallow water solitons are qualitatively similar. Geophysical observations are badly needed to determine whether these results are realistic for the natural world.

3. Methods

3.1. Site

[43] Observations of internal wave interactions were made in the Strait of Georgia, British Columbia. The Strait of Georgia is a large marine waterway on the west coast of North America (Figure 3). It is partially enclosed by islands with Vancouver Island forming the western boundary, and a complex of small islands and channels marking its southern boundary. The Strait of Georgia is about 220 km long and 33 km wide with an average depth of 150 m, but with a small fraction of the total area exceeding 350 m in depth. Depths in the regions observed in this study are greater than 120 m.

[44] Stratification is typical for fjord-type estuaries, with a large density gradient near the surface, little or no uniform mixed layer, and relatively weak stratification at depth [*Pawlowicz et al.*, 2007]. The main source of freshwater maintaining this stratification is the Fraser River. This river discharges near the main entrance of the Strait of Georgia and its turbid plume dominates the southern strait especially in late spring and early summer [*Halverson and Pawlowicz*, 2008]. However, our observations were generally taken away from the direct influence of the plume.

[45] In the southern Strait of Georgia large internal wave "slicks" are regularly observed [*Shand*, 1953; *Turner*, 1973; *LeBlond and Mysak*, 1978; *Hughes and Gower*, 1983]. This visibility is enhanced by the relatively calm and sunny conditions that often occur for periods of several days within the strait during summer, separated by short periods of more windy conditions in which the internal wave surface features cannot be reliably viewed. Thus, the Strait of Georgia is a useful natural laboratory for studying internal waves using optical techniques.

Figure 4. A sample of the original photo images taken on June 26 (interaction Case A). On the image is an oblique top view of two internal wave packets interacting obliquely. A third packet resulting from the interaction is also visible. Slicks are spaced about 200 m apart. The red dot at the center left is the hovercraft.

[46] Many observed internal waves in the Strait of Georgia are concentrated near the surface, with maximum depressions of up to 7 m for isopycnals whose undisturbed depth, within the gradient between the surface brackish water and deep saline seawater, is less than 5 m. These internal waves are often found to be far apart and can be treated as solitary waves [*Wang and Pawlowicz*, 2011]. The length scale across the wave crest is of order 50 m, and the wave crests themselves can sometimes stretch for 10–20 km across the strait. It is this near-surface location that results in large near-surface currents, which, in turn, creates areas of enhanced or reduced roughness, regularly visible to the naked eye. These internal waves often appear in packets, with largest amplitude waves in front, followed by successively smaller waves. The measured phase speeds of these waves range from about 0.6 to 1.2 m s^{-1} [*Wang and Pawlowicz*, 2011].

[47] The tide has a maximum range exceeding 4 m in the Strait of Georgia. Although tidal currents can be greater than 1 m s^{-1} in some of the constricted southern passages (in which the internal waves are formed), they are generally no more than a few 10s of cm s^{-1} within the strait itself [*Foreman et al.*, 1995]. Thus measured internal wave propagation speeds relative to the geostationary frame of reference should be corrected for tides, but the correction is not large.

3.2. Observational Technique

[48] In order to study the oblique interaction of two solitary-like internal waves it is desirable to measure the speed and amplitude of both waves, as well as the spatially and temporally-varying structure near the interaction point. In previous papers, we have described an observational technique that was used to measure the phase speed and internal structure of single waves over a period of about an hour in the Strait of Georgia [*Pawlowicz*, 2003; *Wang and Pawlowicz*, 2011]. Here, the technique is adapted to measure the interaction of two individual wave crests in the region of observation.

[49] The spatial structure of the waves is obtained by photogrammetrically rectifying oblique digital photographic images obtained from an aircraft circling at an altitude of about 400 m. These images (e.g., Figure 4) are obtained at intervals of roughly every1 or 2 minutes for a period of between 30 minutes and an hour. Rectification (e.g., Figure 5) requires accurate estimates of camera location and orientation. Details of photogrammetric rectification of photo images can be found in *Wang and Pawlowicz* [2011]. Although location is relatively simple to determine using GPS logging, camera orientation was measured using a compass/tilt-meter that was affected by the accelerations occurring when aircraft orientation was changing rapidly, and hence not all photos can be used. In addition, the surface reflectance also varies with the horizontal viewing angle. Often images from only part of the track are useful. However, phase speeds were measured to an accuracy of about 10% [*Wang and Pawlowicz*, 2011], and wave locations to an absolute accuracy of less than 100 m.

[50] Water column information was provided by deploying equipment from a hovercraft that could be rapidly directed to an interaction region by radio command from the aircraft once a wave interaction was located. Measurements obtained using the hovercraft included CTD (Conductivity-Temperature-Depth) profiles (Figure 6), ADCP (Acoustic Doppler Current Profiler) current profiles, echo sounding of

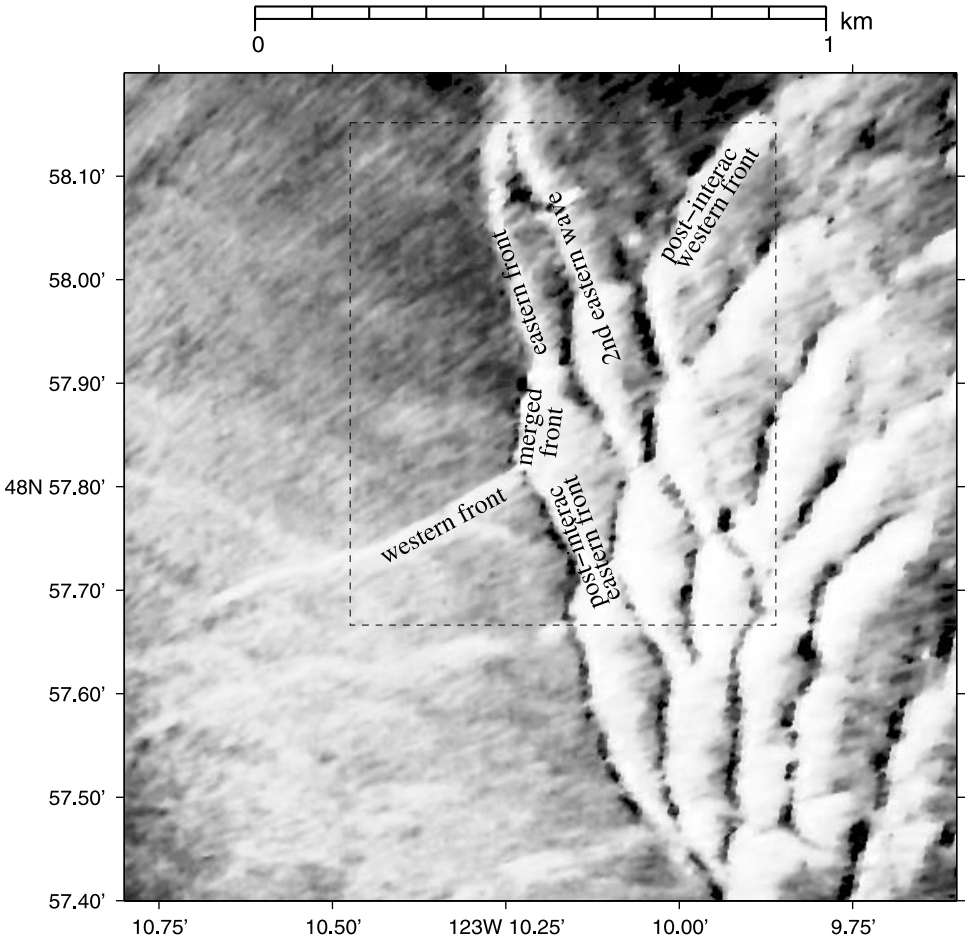

Figure 5. A rectified and processed version of the image in Figure 4 (Case A). This image was taken when the aircraft was to the southwest of the observed waves. In the image, there are three wave packets. The dashed box shows the area covered by the schematic of Figure 7.

small density interfaces embedded in the thermocline, and thermistor string (T-chain) measurements for high-spatial resolution views of the wave structure.

[51] Angles between wave normals and the wave amplitudes are required in order to study oblique interactions. Angles between waves are measured on the processed images bearing the appropriate interaction pattern. The wave amplitudes are provided by the water column data [*Wang and Pawlowicz*, 2011]. For certain waves water column data are not available. In these cases estimates of wave amplitudes are obtained based on the measurements of propagation speeds, which are made by analyzing the image sequences and subtracting tidal effects, as in *Wang and Pawlowicz* [2011].

4. Results

[52] Observations were obtained during "day trips" in 2001 and 2002, occurring every week or so through the summer in 2002. Interaction patterns were observed on 4 occasions (June 10, 25, 26, and July 15 of 2002). Largest density changes are confined to the upper 20 m. Densities decrease rapidly in the upper 5 m (Figure 6).

4.1. Case A

[53] A wave-wave interaction (Figures 4 and 5) was observed near Point Roberts on June 26 and will be studied first in detail as an example. Subsequent cases will be discussed more briefly.

[54] Photo images taken between 15:20 and 15:50 bearing the same interaction pattern (Figure 5) are used. The three wave packets are named by their geographical positions as the western packet, the eastern packet, and the merged packet. As shown in Figure 5, the western packet stands for the wave packet on the western side (left side) of the three wave packet pattern, and its wavefront is then called the "western front". The eastern packet stands for the wave packet on the eastern side (right side) and its wavefront is called the "eastern front". The wave packet generated due to the interaction of the western and eastern packets is located in the middle of the two interacting wave packets and is called the merged packet. Its leading wave is named as the "merged front". The western packet is composed of at least three visible waves, although surface expressions are much more visible after the interactions. The eastern packet has two visible waves. The wave labeled as "2nd eastern wave" is the second wave in the eastern packet.

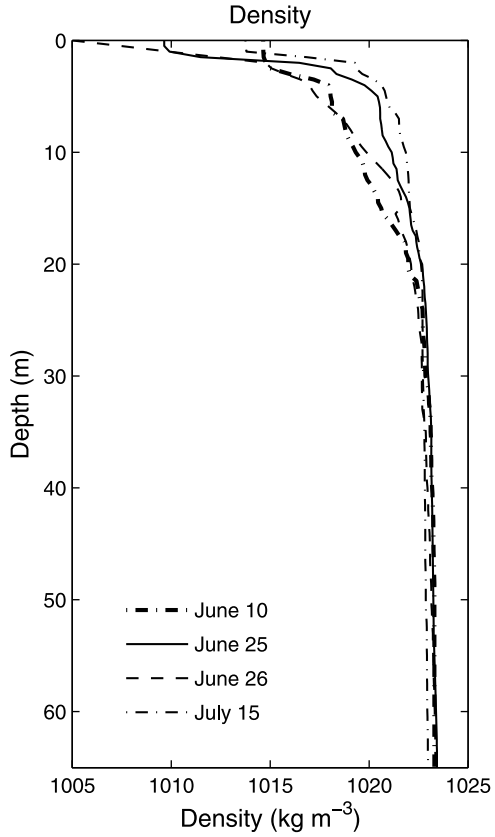

Figure 6. Density profiles for the studied cases. Only the top 70 m are shown.

[55] Figure 7 is a schematic redrawn of the wave crests in Figure 5 in order to better analyze the wave-wave interaction. The western front travels to the northwest in the direction of 60° to the north from west (tidal effects subtracted). The eastern front propagates to the southwest with an angle of 23° south of west. The merged front due to the interaction is traveling to the west and has an angle of 4° to the north of west. The interaction angle between the western front and the eastern front is therefore 83°. The angles between the leading front of the eastern and the western packets and the merged front are measured as 28° and 55°, respectively. The angle between the post-interaction eastern front and the merged front is 40°. The angle between the post-interaction western front and the merged front is not easy to identify because it has also interacted with the second wave of the eastern wave packet, but appears to be approximately (50 ± 20)°. Wave crests after interaction are not parallel to their original positions. The post-interaction eastern front was rotated 12° counter-clockwise. The post-interaction western front was rotated in the range of [−25° 15°] clockwise.

[56] There are only two waves visible in the eastern packet of this image. The second wave has larger amplitude (3.8 ± 0.3 m) than the leading wave (2.3 ± 0.1 m). Thus it will eventually overtake the leading wave, but over the time period of our observations the collision does not occur. Since we are looking at the interaction over a period of about 30 minutes, it is not unreasonable to assume that the post-interaction western front is affected mainly by interaction between the western packet and the larger wave of the eastern packet. The amplitude of the post-interaction western front is 3.3 ± 0.3 m. Since the measured phase speed of the western front and the post-interaction western front are similar (≈0.5 ± 0.1 m s^{-1}), it is assumed that the amplitude of the western front is also approximately 3.3 ± 0.3 m.

4.2. Case B

[57] On July 15 an interaction similar to Case A was observed close to Point Roberts between a northward propagating wave packet and a westward propagating wave packet (Figure 8). The packet on the right-hand or northeast side is called the eastern wave packet while the other packet on the left or southwest is called the western wave packet. Similar to Case A, as shown in Figure 8, waves are named as "western front", "eastern front", "merged front", "post-interaction western front", and "post-interaction eastern front". A phase diagram (Figure 9) was created based on the image in Figure 8. The western front was propagating to the north with an angle of 80° from the east. The eastern front was propagating to the southwest and had an angle of 6° from the west. The merged front was propagating to the northwest with an angle of 35° from the west. The interaction angle between the two wave normals of the western and eastern fronts is ψ = 98°. The angle between the western front and the merged front is 60°, the angle between the eastern front and the merged front is 37°, the angle between the post-interaction eastern front and the merged front is 42°, the angle between the post-interaction western front and the

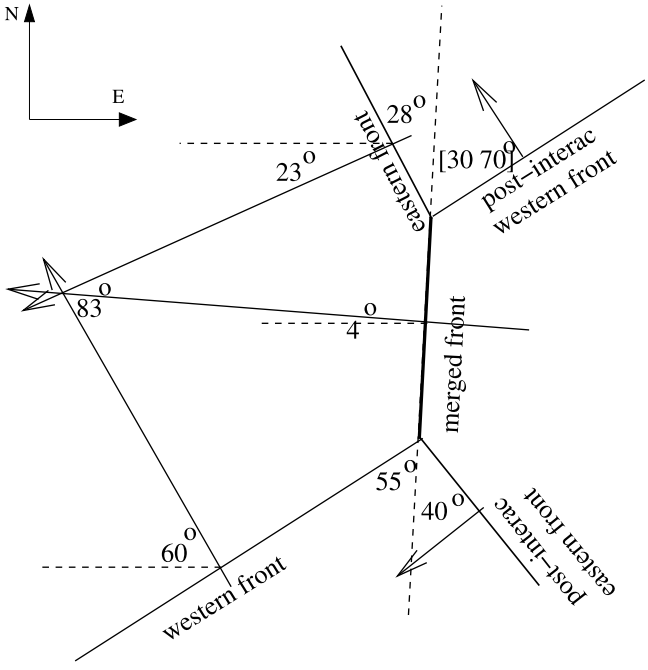

Figure 7. A cartoon of the interacting wavefronts and their individual propagation direction for the interaction Case A observed on June 26. The western front and the eastern front interact and a third wave, the merged front, is generated between them. The merged front travels in between the propagation directions of the two interacting waves.

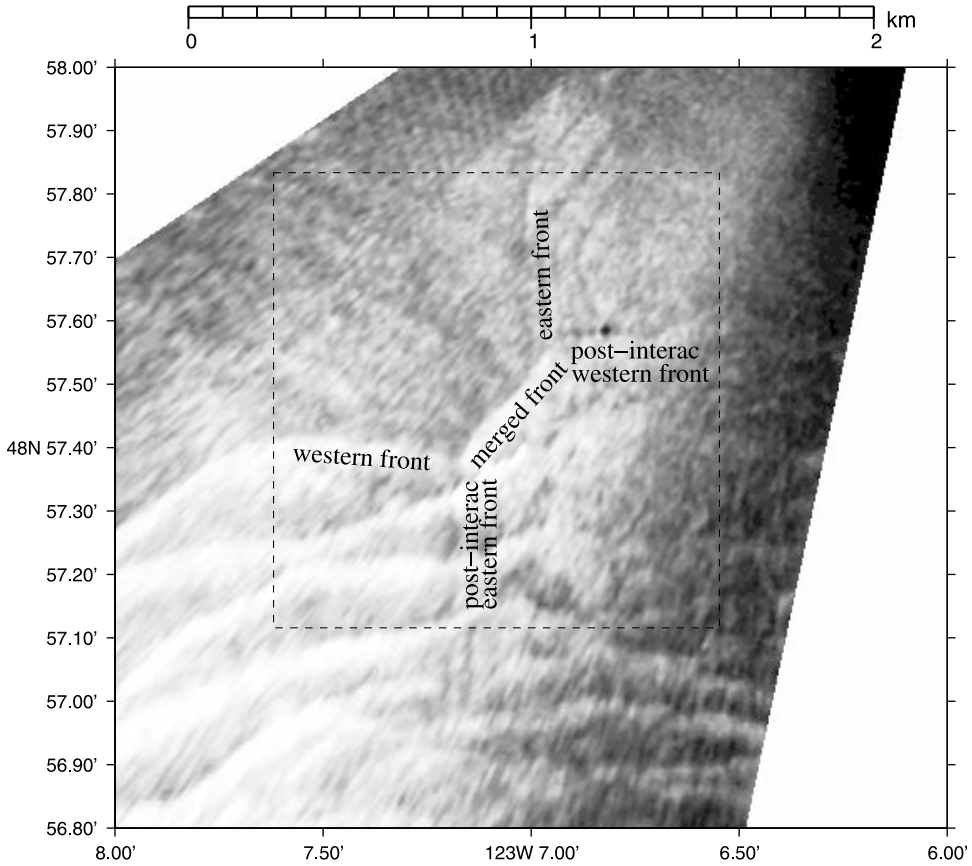

Figure 8. Image of the interaction pattern Case B observed on July 15. This image was taken from the northeast. There are three wave packets observed.

merged front is 66°. The post-interaction eastern front is rotated 5° relative to eastern front and the post-interaction western front is rotated 6° relative to the western front.

[58] The amplitude of the eastern wavefront is 4 ± 0.4 m and the amplitude of the western wavefront is 3.8 ± 0.4 m. The amplitude of the post-interaction western front is measured with water column data as 3.2 ± 0.2 m. The amplitude of the post-interaction eastern front was not directly measured and its phase speed can not be easily estimated because of difficulties in identifying it in a time sequence of the available photo images.

4.3. Case C

[59] On June 25 an interaction pattern that resembles Case A and Case B but without any merged front seen was also observed near Point Roberts. The interaction is between a western propagating packet and a northwestern propagating wave packet (Figure 10). The hovercraft sampled the second wave of the eastern wave packet instead of the leading front. Hence, this case study will be about the interaction between the western front and the second wave of the eastern packet, the "eastern wave". The interaction angle between the two wave normals is $\psi = 60°$. The observed wave amplitudes are especially large. The eastern wave has an amplitude of 4.6 ± 0.4 m and the western wavefront has an amplitude of 6 ± 0.3 m.

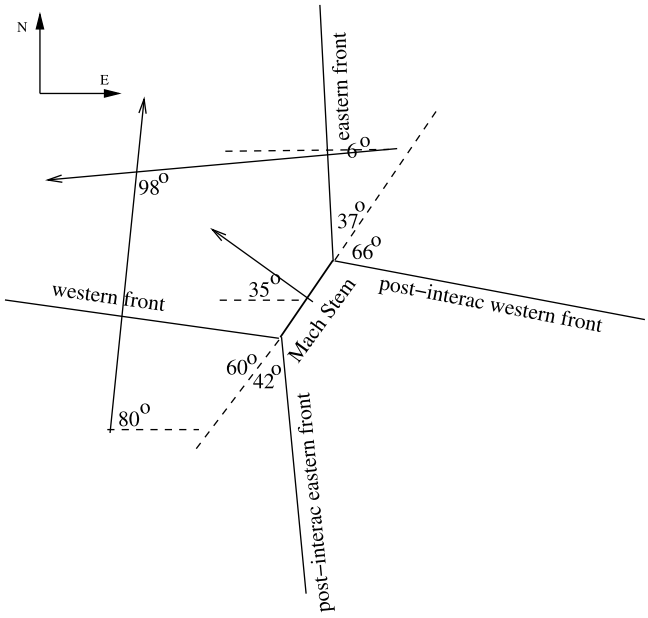

Figure 9. The diagram of wave-wave interaction Case B on July 15 based on Figure 8. The western front and the eastern front interact and a third wave, the merged front, is generated between them. The merged front travels in between the propagation directions of the two interacting waves.

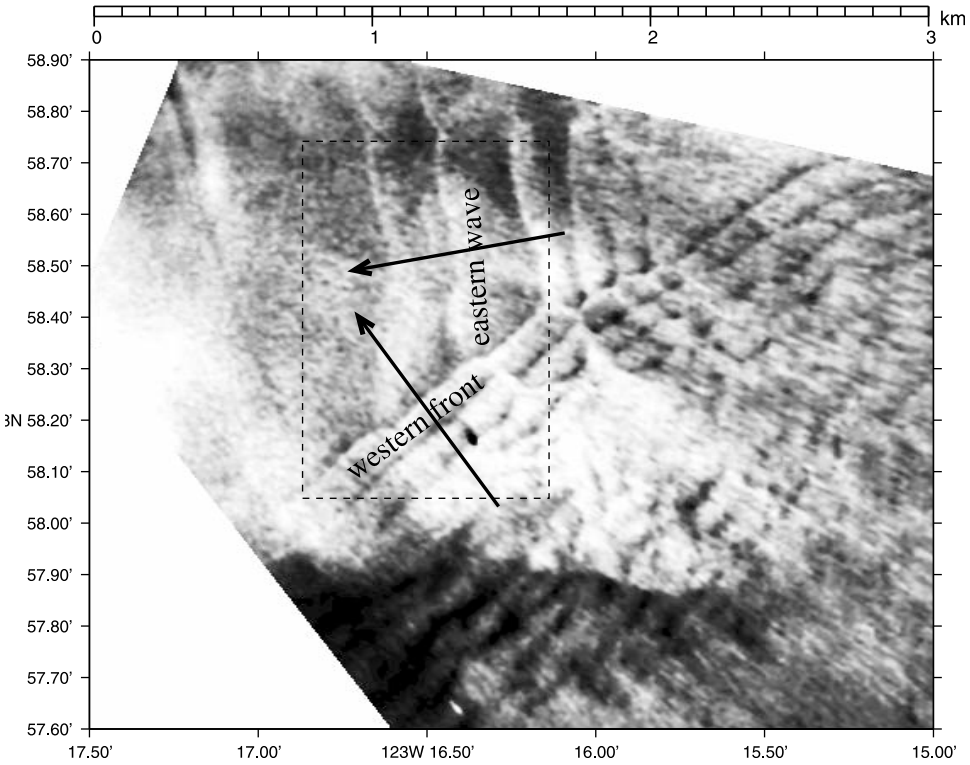

Figure 10. The interaction pattern Case C on June 25.

4.4. Case D

[60] Although the previous cases have shown interactions at relatively large angles, the interactions at shallow angles, especially when wave amplitudes differ (case 2 in Figure 1), are interesting because they are very similar to the well-known 1-D interactions. One aspect of 1-D interactions is that the two wave crests may seemingly never merge. Instead the surface height field has the appearance of one crest "pushing away" the other. On June 10, this kind of pattern (Figure 12) was observed.

[61] Our water column data suggests the two waves have a length scale of about 150 m and the distance between two troughs of the same wave is about 260 m. The closest approach of the crests is about 160 m which would suggest some interaction is occurring. This appears to be an oblique wave-wave interaction with a very small interaction angle (case 2 in Figure 1). The interaction angle between the two wave normals is $\psi = 10°$. A cartoon of this interaction is shown in Figure 13. The waves are named as the first wave, second wave, post-interaction first wave, and post-interaction second wave.

[62] The water column data can only provide the amplitudes of the post-interaction second wave (3 ± 0.2 m) and the first wave (2.9 ± 0.3 m). Assuming that the second wave does not experience significant modifications to its wave properties, especially amplitude, during this interaction this value is used for the pre-interaction second wave as well.

5. Analysis and Discussion

[63] Interaction patterns that include a "bar" between the two waves (case 3 or 4 in Figure 1) were observed on both June 26 (Case A) and July 15 (Case B). On June 25, the observed interaction (Case C) falls into the parameter range of Mach interaction (case 3 in Figure 1), but there is no Mach stem observed. On June 10 (Case D), the observed interaction pattern resembles case 2 of Figure 1, with a very

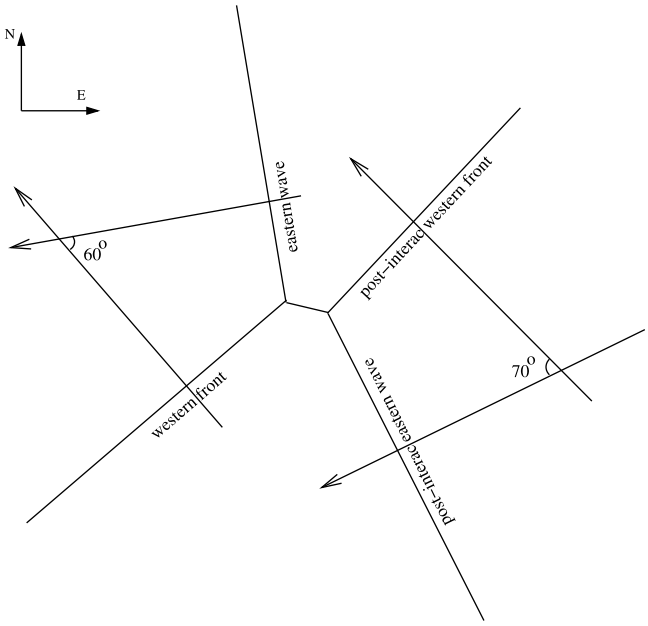

Figure 11. Interaction diagram of interaction Case C generated based on Figure 10. The western front and the eastern wave interact with an interaction angle of 60°. Instead of a Mach stem between two interacting waves, there is a runup generated behind the joining point of them.

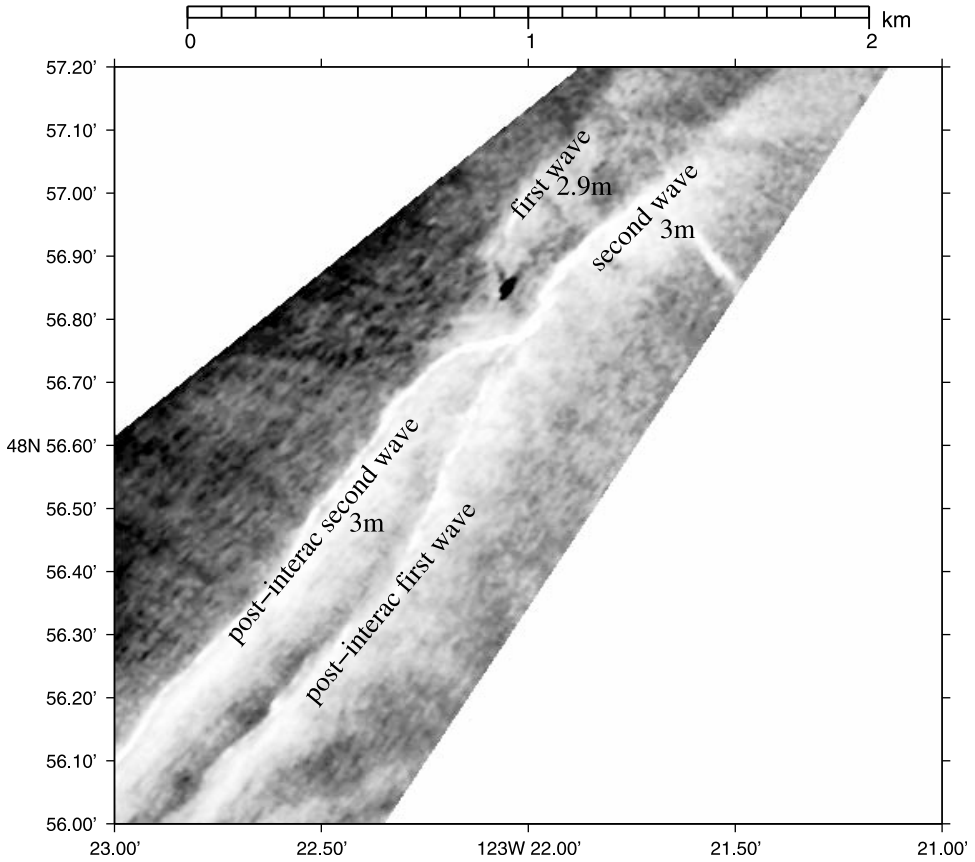

Figure 12. Image of wave-wave interaction Case D on June 10. Second wave propagates faster than first wave. After interaction, second wave jumps forward, while first wave shifted backward.

shallow interaction angle and relatively large amplitude difference. One wave suffered a negative phase shift, another wave experienced a positive phase shift, and the total phase was conserved.

[64] Note that the internal solitary-like waves observed in the Strait of Georgia are not "small amplitude", because the wave displacements are of the same order as the effective depth. However, the waves are far from having maximal amplitude [*Wang*, 2009]. These waves are not shallow water waves, because their length scales are short relative to the depth of the deep water below the pycnocline, and background shear is present. However, in *Wang and Pawlowicz* [2011], it was shown that there was little difference in the propagation speeds predicted by weakly nonlinear and maximal amplitude theories for these waves and it is possible the same is true for interactions. Therefore, it is reasonable to begin a comparison using existing theory.

[65] In this section, the observed interactions are first qualitatively classified according to the cases in Figure 1 and then more detailed comparisons with *Miles* [1977] theory for Mach interactions are made. The measured values including wave amplitudes and the angles between waves will allow for quantitative comparison. The amplitudes must be nondimensionalized and this is done by dividing the amplitudes by h_{eff}. For simplicity we take this to be the depth of the maximum value of Buoyancy frequency, which is obtained based on the observed continuous stratification. In our situation, h_{eff} is found to lie in the range of [2 4] m.

5.1. Analysis of Observed Interactions

5.1.1. Case A

[66] For Case A observed on June 26, $\eta_1 = 3.3$ m (western front), $\eta_2 = 3.8$ m (eastern wave), and $\psi = 1.4$ (i.e. 83°). Thus

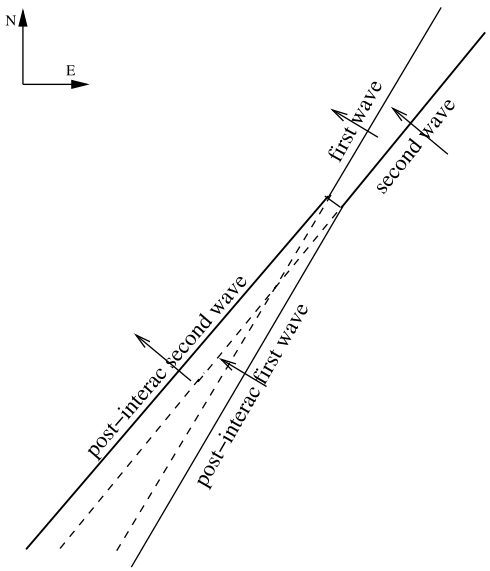

Figure 13. Diagram of wave-wave interaction Case D on June 10.

by dividing the effective depth h_{eff} ([2 4] m) the nondimensional wave amplitudes are obtained in the range of $\eta_1' = [\mathbf{0.8}\ 1.6]$ and $\eta_2' = [\mathbf{0.9}\ 1.9]$. The amplitudes nondimensionalized by $h_1 = 4$ m are highlighted with bold text.

[67] First, the interaction can be viewed as a reflection (i.e. a symmetric interaction) since $|\eta_2' - \eta_1'| < \psi^2$ is satisfied, although in fact it is not quite geometrically symmetric. The eastern front has larger amplitude than the western front and experiences a smaller phase shift, while the western front with smaller amplitude suffers a larger phase shift, resulting in the observed asymmetry. This agrees with the line drawing on the right side of Figure 1.

[68] Second, since $|\eta_2' - \eta_1'| < \psi^2$ the interaction is not predicted to be phase-conserving and this agrees with the observed forward phase shift of both interacting waves as we can see from Figures 5 and 7.

[69] Third, $\left(\frac{\psi}{2}\right)^2 = O(\eta_{1,2}')$ is satisfied suggesting it is a strong interaction, and this can be confirmed by the magnitude of the large spatial shifts in wave crests caused by the interaction. As shown in Figure 5, the displacements in the direction of wave propagation between the post-interaction western front and the western front, and between the post-interaction eastern front and the eastern front are around 100–200 m, comparable to horizontal wave scales. Also, as will be shown later, this interaction lasts for a quite long time (over one hour) while the timescale of the particles moved by the waves is only several minutes.

[70] Fourth, a regular interaction is predicted to become a Mach interaction when $\psi_- < \sin^2\frac{\psi}{2} < \psi_+$ and $\psi_\pm = \frac{3}{4}(\sqrt{\eta_1'} \pm \sqrt{\eta_2'})^2$, i.e. when equation (1) is satisfied. Here, $\psi = 1.4$, $\sin^2\frac{\psi}{2} = 0.4$, $\psi_- = [\mathbf{0.003}\ 0.006]$, and $\psi_+ = [\mathbf{2.6}\ 5.3]$, so it is well within the theoretical Mach interaction regime. The crest length of the merged front is observed to grow slowly with time with a step angle of $(3.3 \pm 2.5)^\circ$. Since the stem length increases with time and this is one unique characteristic of a Mach interaction differing from a regular interaction, this observed case is most probably a Mach interaction. However, it is also possible that this growth rate occurs as a transient related to the finite length of the crest of real waves. We do not have any further data to address this issue.

[71] Since there are no direct measurements of the wave amplitudes for Mach stem and the post-interaction waves, these are estimated from wave phase speed observations and the amplitude measurements of other waves using a heuristic rule that a larger amplitude wave has faster wave speed than a smaller wave under the same conditions. The observed wave speed of the Mach stem (0.77 ± 0.1 m s^{-1}) is larger than any of the other waves (0.52 ± 0.08 m s^{-1} and 0.55 ± 0.05 m s^{-1} for the western front and the eastern front, respectively), therefore, the estimated amplitude for the Mach stem is larger than 3.3 ± 0.3 m but less than double this value.

[72] The apparent origination time of the Mach stem can also be estimated by extrapolating backwards in time from the measured growth rate and the present size of the stem. The apparent origination time is found to be around 14:20 or about one hour before our observations. Therefore, we infer that the time length for the full development of the Mach interaction is longer than one hour. This is much longer than the timescale (wavelength/wave speed) of particles in the observed waves which is several minutes. The observed long maturing time also agrees with *Funakoshi* [1980, 1981] who suggested that Mach reflection is a much slower process than a regular reflection, and that it generally takes a long time for the asymptotic situation to be achieved.

5.1.2. Case B

[73] For Case B observed on July 15, the dimensionless amplitudes are $\eta_1' = [\mathbf{0.95}\ 1.9]$ (western front) and $\eta_2' = [\mathbf{1}\ 2]$ (eastern front). The interaction angle between two wave normals is $\psi = 1.71$ (98°).

[74] First, $|\eta_2' - \eta_1'| < \psi^2$ is satisfied and this suggests that this interaction can be treated as a symmetric interaction (reflection). Again it is not exactly symmetric, even though the amplitudes are similar enough that it can be treated as a reflection. The asymmetry is caused by the difference between the interacting wave amplitudes.

[75] Second, the interaction angle ψ satisfies $\sin^2(\psi/2) = 0.57$, which is less than $O(\eta_{1,2}')$, suggesting it is a strong interaction.

[76] Third, $|\eta_2' - \eta_1'| < \psi^2$, also suggesting that this interaction is not phase-conserving. This agrees with the observed forward phase shifts of both of the two interacting waves near the interaction as shown in Figures 8 and 9.

[77] Fourth, again it is easy to find that for this interaction case equation (1) is satisfied. Since this case is a reflection problem it can also be examined as a reflection using equation (3). The eastern wavefront with greater amplitude is taken as the incident wave and the post-interaction western front as the reflected wave. The incident angle is half of the interaction angle, which is $\psi_i = \frac{\psi}{2} = 49^\circ$ (≈0.86) and the incident amplitude is $\eta_i = 4$ m ($\eta_i = [\mathbf{1}\ 2]$). It is found that $\psi_i/(3\eta_i')^{1/2} \leq 1$, i.e. it is a Mach reflection.

[78] The speed of the Mach stem is again greater than the speed of the western and the eastern front. Therefore, the Mach stem's amplitude must be larger than the western and the eastern wavefront, i.e. greater than 4 m. The Mach stem step angle is estimated to be $10^\circ \pm 5^\circ$. The non-zero step caused by the growth of stem length again suggests that this is a Mach interaction. This Mach interaction began around 15:15 about one hour before it was observed. Similar to Case A, this long interaction time (greater than wave timescale) and the spatial displacements between pre- and post-interaction waves (greater than wavelength scale) again indicate the strong interaction nature of this case.

5.1.3. Case C

[79] As shown in Figure 11 for the interaction pattern observed on June 25 (Figure 10), the interaction angle between the two wave normals is $\psi = 1.05$ (60°). The dimensionless amplitudes are $\eta_1' = [\mathbf{1.1}\ 2.3]$ and $\eta_2' = [\mathbf{1.5}\ 3]$. First, $|\eta_2' - \eta_1'| < \psi^2$ implying that this case can be treated approximately as a reflection problem. Second, the satisfaction of this criterion also means that for this interaction the phase is not conserved. Third, it is a strong interaction since $\psi^2 = O(\eta')$. Fourth, we also have $\frac{3}{4}(\sqrt{\eta_2'} - \sqrt{\eta_1'})^2 < \sin^2(\psi/2) < \frac{3}{4}(\sqrt{\eta_2'} + \sqrt{\eta_1'})^2$, so it is possible that this case is a Mach interaction problem. However, no Mach stem is observed, so the interaction pattern as shown in Figure 10 does not resemble a Mach interaction.

Table 1. Interaction Case A on June 26[a]

Parameter $\varepsilon \equiv \frac{\psi}{2}/\sqrt{3\eta_i'}$	Theory		Observation
	$\varepsilon \geq 1$ Regular Reflection (Small Amplitude)	$\varepsilon < 1$ Mach Reflection (Small Amplitude)	ε = [0.3 0.4] (Large Amplitude)
Step angle ψ_*	0	$\sqrt{\frac{1}{3}\eta_i'}\ (1-\epsilon)$ ([**19** 32]°)	4° ± 2.5°
Interaction amp. η_M	non-grazing (maximum runup) ([**13** 18] m)	$(1+\varepsilon)^2\eta_i$ (Mach stem)([6.4 **7.4**] m)	>3.8 m (based on wave speed observations)
Reflected wave amp. η_r	η_i (3.8 m)	$\varepsilon^2\eta_i$ ([0.33 **0.66**] m)	≈3.3 m
Reflection angle ψ_r	ψ_i (42°)	$\sqrt{3\eta_i'}$ ([97 **137**]°)	(45 ± 10)°

[a]See text for explanation of the bold values in Tables 1–3.

5.1.4. Case D

[80] From the schematic of this interaction (Figure 13), the interaction angle between the two wave normals is ψ = 0.18 (10°). The nondimensional wave amplitudes are η_1' = [**0.73** 1.45] for the first wave and η_2' = [**0.75** 1.5] for the second wave. The observed values are again applied to the classification criteria and it is found that this interaction is not symmetric, it is a strong interaction, phase is conserved, and it is not a Mach interaction. This is case 2 in Figure 1 with the second wave obliquely overtaking the first wave. The first wave is shifted backward while the second wave shifted forward, so the total phase is conserved.

5.2. Discussion on Cases in Mach Interaction Parameter Range

[81] The interactions observed on June 26 (Case A), July 15 (Case B), and June 25 (Case C) are re-examined and compared with the available theory of *Miles* [1977] more quantitatively because although these wave cases fall in the parameter domain of Mach interaction their appearances differ in some respects from a Mach interaction.

[82] If case A treated as a Mach reflection, the incident angle is ψ_i = 0.7 (42°), and the nondimensional incident amplitude is η_i' = [**0.9** 1.9]. The reflected angle (half of the angle between the wave normals of the two post-interaction waves) is approximately $\psi_r = 0.8 \pm 0.17 \left(i.e. \frac{(50\pm20)^\circ+40^\circ}{2} = (45 \pm 10)^\circ\right)$. Due to the uncertainty of the angle between the post-interaction western front and the Mach stem, there is an error of the value of the reflected angle ψ_r as well. Using these values we compute various parameters for both regular and Mach reflection cases, and compare them with observations (see the first three columns of Table 1). The computation of the parameters in Table 1 are based on the formulas summarized in section 2. Observations of these parameters are in the last column of Table 1.

[83] The comparison of the interaction as shown in Table 1 does not match either regular or Mach reflection predictions, but the differences are consistent with those described by *Tanaka* [1993] for larger amplitude waves and can be summarized as follows:

[84] 1. The observed Mach stem step angle is significantly greater than zero and it is smaller than the theoretical value of a Mach reflection case.

[85] 2. The observed Mach stem amplitude is smaller than the runup in a regular reflection case and closer to the theoretical Mach stem amplitude.

[86] 3. The observed reflected wave amplitude lies between the theoretical values of regular and Mach reflections.

[87] 4. The observed reflection angle appears to be smaller than its value if treated as a theoretical Mach interaction and greater than the theoretical regular reflection although there is an uncertainty associated with estimating the reflection angle ψ_r.

[88] Overall, the observed reflection characteristics for the observed large amplitude waves deviate from those of the theoretical small amplitude Mach reflection toward those of the theoretical regular reflection. The degree of agreement depends somewhat on the h_{eff} used in nondimensionalization. The weaker the nonlinearity i.e. the deeper the depth of h_{eff} (highlighted as bold characters), the closer the results to the theoretical values of weakly nonlinear Mach reflection. The stronger the nonlinearity (decreasing h_{eff}), the closer the results are to those of a regular reflection. We hypothesize that the above deviations from the weakly nonlinear Mach reflection are caused by the strong nonlinearity i.e. the large nondimensionalized amplitudes of the waves involved. Although this case has stronger nonlinearity ($\eta' \approx 1$) than Tanaka's [*Tanaka*, 1993] numerical model, where η' = [0.1 0.3], our results agree with his numerical results stating that the effect of large amplitude tends to prevent the Mach reflection from occurring. Even when a Mach reflection occurs, it is "contaminated" by regular reflection [*Tanaka*, 1993].

[89] The comparison of the second presumed Mach interaction Case B observed on July 15 (Figure 8) with *Miles*

Table 2. Interaction Case B on July 15

Parameter $\varepsilon \equiv \psi_i/\sqrt{3\eta_i'}$	Theory		Observation
	$\varepsilon \geq 1$ Regular Reflection (Small Amplitude)	$\varepsilon < 1$ Mach Reflection (Small Amplitude)	ε = [0.35 **0.5**] (Large Amplitude)
Step angle ψ_*	0	$\sqrt{\frac{1}{3}\eta_i'}\ (1-\varepsilon)$ ([**17** 30]°)	10° ± 5°
Interaction amp. η_M	non-grazing (maximum runup) ([**11** 14] m)	$(1+\varepsilon)^2\eta_i$ (Mach stem)([7 **9**] m)	>4 m (based on wave speed observations)
Reflected wave amp. η_r	η_i (4 m)	$\varepsilon^2\eta_i$ ([0.5 **1**] m)	3.2 m
Reflection angle ψ_r	ψ_i (49°)	$\sqrt{3\eta_i'}$ ([99 **140**]°)	54°

Table 3. Interaction Case C on June 25

Parameter $\varepsilon \equiv \psi_i/\sqrt{3\eta_i'}$	Theory: $\varepsilon \geq 1$ Regular Reflection (Small Amplitude)	Theory: $\varepsilon < 1$ Mach Reflection (Small Amplitude)	Observation: ε = [0.35 **0.5**] (Large Amplitude)
Step angle ψ_*	0	$\sqrt{\frac{1}{3}\eta_i'}\,(1-\varepsilon)$ ([**21** 37]°)	0
Interaction amp. η_M	non-grazing (maximum runup) ([**43** 75]m)	$(1+\varepsilon)^2\eta_i$ (Mach stem)([11 **13**]**m**)	not available
Reflected wave amp. η_r	η_i (6 m)	$\varepsilon^2\eta_i$ ([0.7 **1.5**]m)	not available
Reflection angle ψ_r	ψ_i (30°)	$\sqrt{3\eta_i'}$ ([122 **172**]°)	35°

[1977] is very similar to the case on June 26 as we can see from Table 2. This Mach reflection is also contaminated by regular reflection because of the strong nonlinearity of the interacting waves. The observed Mach stem step angle, the reflected wave amplitude, and the reflection angle are all smaller than the theoretical values of a pure Mach reflection.

[90] We can also compare our observations with the numerical experiments of *Tsuji and Oikawa* [2001] who numerically studied some cases of deep water internal wave interactions. Their main results are summarized as: with incident wave amplitude $\eta_i' = 2$ (nondimensionalized by the thinner layer depth), the critical angle for Mach reflection is $\psi_c = 59°$, i.e. it is Mach reflection if the incident angle $\psi_i < 59°$ (for the weakly nonlinear theory this critical angle occurs when $\eta_i' = \psi_i^2/3 \approx 0.3$) and the maximum stem amplitude occurs when $\psi_i \approx \psi_c$, i.e. close to the critical angle. The incident angles of Case A and Case B are both smaller than the critical angle of 59° found by *Tsuji and Oikawa* [2001] for $\eta_i' = 2$, therefore, this suggests that the observed interaction could still qualify to be a Mach interaction under the circumstance of strongly nonlinear and deep water waves. At our observed amplitude of $\eta_i' \approx 1$ the measured incident angles of 42° (Case A) and 49° (Case B) must be close to critical.

[91] The observed asymmetry in angles between the stem and the two original waves (Figure 7) is caused by the differences in amplitude between the two interacting waves. According to the analytical results of *Matsuno* [1998] studying oblique interaction in a deep-fluid system, to leading order the phase shift does not depend on the amplitude, but in the second order it is proportional to the amplitude of the other wave. For our large wave amplitudes, the second order is important and can not be neglected. Therefore, it might be expected that the phase shift of the smaller wave (western front) is greater than the larger wave (eastern wave). Our observations showed that not only do the distances between the post-interaction and the original waves depend on each other's wave amplitudes, the direction rotations due to a Mach interaction are also related to the other wave's amplitude. The larger wave (eastern wave) is rotated a smaller angle than the smaller wave (western front). Due to the combination of the asymmetric phase shifts and direction rotations, the Mach stem is inclined to the direction of the larger wave and causes the observed asymmetry.

[92] Although there is no Mach stem observed, Case C (Figure 10) is also studied as a reflection problem. The western front with the greater amplitude is taken to be the incident wave. The post-interaction eastern wave is the reflected wave. The incident wave amplitude is η_2' and the reflected wave amplitude is η_1'. The incident angle is half the interaction angle, $\psi_i = 30°$, and the reflection angle is $\psi_r = 35°$. The asymmetry is again caused by the different wave amplitudes of the interacting waves. The comparison results are shown in Table 3. Surprisingly, the comparison is not dramatically different from comparisons we did for Case A and Case B even though the interaction pattern seems much different. However, recall that the theoretical values for either regular or Mach reflection are meant to work only for waves with very small wave amplitudes. The comparison with Miles' small amplitude theory can only tell us that our observations of large waves lie somewhere in between regular reflection and Mach reflection despite its appearance of a regular reflection or Mach reflection. With $\psi_i < \psi_c\ (= \sqrt{3\eta_1'})$ satisfied, this case is inside of the Mach reflection regime of Miles. However, recalling the definition of Mach stem, "the apex of the incident and the reflected waves moves away from the wall at a constant angle (stem angle) and is joined to the wall by a solitary wave called Mach stem" [*Tanaka*, 1993], there is no Mach stem observed in this case. We are not alone with this finding. In *Tanaka* [1993], a numerical experiment was carried out for $\eta_i = 0.3$ and $\psi_i = 40°$, and it was found that the stem length did not grow and $\eta_r = \eta_i$, which indicated that it was actually a regular reflection rather

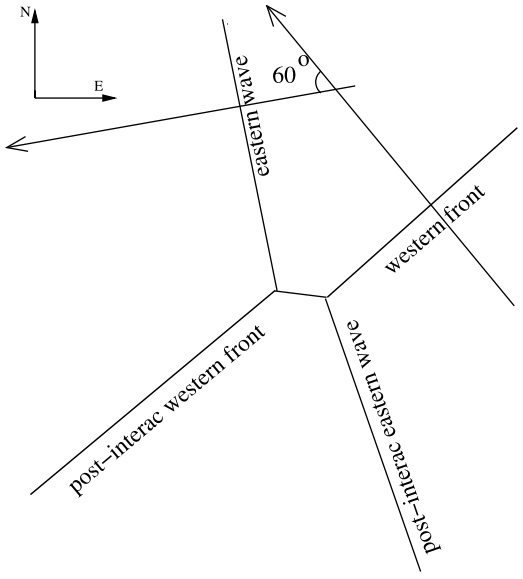

Figure 14. The interaction pattern on June 25 can also be viewed as case 2 of Figure 1. The western front and the eastern wave interact. After interaction, the western front is shifted forward and the eastern wave is shifted backward.

than a Mach reflection even though $\psi_i/\sqrt{3\eta_i'} = 0.736 < 1$. Therefore, even when the above condition of Miles is satisfied, when the wave amplitudes are large enough, a Mach interaction may not occur. Correct predictions in large amplitude cases clearly require a more sophisticated theory.

[93] A second possibility is that the wave magnitudes and/or the difference in wave amplitudes may be large enough that the above Miles' criteria of phase conserving, reflection, and Mach interaction are not applicable any more. Therefore, we may be seeing case 2 (obliquely overtaking) of Figure 1. That is, it is fundamentally a shallow-angle interaction with one wave (western front) shifted forward and the other wave (eastern wave) shifted backward as illustrated in Figure 14.

[94] One caveat associated with all of these analyses concerns the issues of refraction or steering by horizontal gradients in background currents and densities. We have assumed that these background density and current fields are approximately constant over horizontal scales of several hundred meters. This seems reasonable since rapid changes over those scales would likely also result in some kind of surface expression which we did not observe in the rectified images. However, further analysis of the lateral curvature of waves over strait-wide scales [*Wang*, 2009] does suggests that refraction and steering effects may play a role in understanding the ultimate positions of these waves after long time periods and over large distances.

6. Conclusion

[95] A number of instances in which strongly nonlinear internal waves interact nonlinearly were measured and analyzed. Although far from being comprehensive, these observations represent the first field measurements of such interactions. Overall, it is found that although the behavior described by a weakly nonlinear analysis (section 2) is qualitatively correct, a detailed comparison shows significant deviations. In particular, when Mach interactions occur, the growth and amplitude of the Mach stem is somewhat less than predicted.

[96] On the other hand, at this level of comparison it is not clear what (if any) difference may be expected between the interactions of shallow water waves as described by KdV-type equations and the interaction of deep water waves described by BO-type equations. Our findings on the limitations of Miles' theory [*Miles*, 1977] are at least consistent with those of *Tanaka* [1993]. Other sources of the discrepancy might also be the strongly nonlinear nature of the interaction. In addition, anecdotal observations of surface wave interactions that are similar to Mach interactions often show breaking in the Mach stem. If enhanced mixing is occurring within these internal wave interactions, then the result could act as a significant sink of energy in the propagation of wave packets. Unfortunately we did not manage to make water column measurements actually in the Mach stem to verify this hypothesis.

[97] In future research on Mach interaction, an effort should be made to track the Mach stem for a longer time, at least several hours, as well as water column measurements within the stem. Measurements over longer timescales may provide a better idea of the process of Mach stem interaction as it reaches its asymptotic state, or indeed if it does reach a steady constant growth rate.

[98] **Acknowledgments.** We wish to thank the crew of the CCGS Siyay for their outstanding assistance in helping us hang instruments off all parts of the vessel, and to the pilots and staff of Harbour Air Seaplanes. This research was supported by the Natural Sciences and Engineering Research Council of Canada under grant 194270-02. This research was also supported by the National Natural Science Foundation of China under grant 41106008 and the State Key Laboratory of Tropical Oceanography (South China Sea Institute of Oceanology, Chinese Academy of Sciences) under grant LED1003.

References

Benjamin, T. B. (1966), Internal waves of finite amplitude and permanent form, *J. Fluid Mech.*, *25*(2), 241–270, doi:10.1017/S0022112066001630.

Foreman, M. G. G., R. A. Walters, R. F. Henry, C. P. Keller, and A. G. Dolling (1995), A tidal model for eastern Juan de Fuca Strait and the southern Strait of Georgia, *J. Geophys. Res.*, *100*(C1), 721–740, doi:10.1029/94JC02721.

Funakoshi, M. (1980), Reflection of obliquely incident solitary waves, *J. Phys. Soc. Jpn. 49*, 2371–2379.

Funakoshi, M. (1981), On the time evolution of a solitary wave reflected by an oblique wall, *Rep. Res. Inst. Appl. Mech. Kyushu Univ. 29*, 79–93.

Grimshaw, R., and Y. Zhu (1994), Oblique interactions between internal solitary waves, *Stud. Appl. Math.*, *92*, 249–270.

Halverson, M. J., and R. Pawlowicz (2008), Estuarine forcing of a river plume by river flow and tides, *J. Geophys. Res.*, *113*, C09033, doi:10.1029/2008JC004844.

Hammack, J., D. Mccallister, N. Scheffner, and H. Segur (1995), Two-dimensional periodic waves in shallow water. Part 2. Asymmetric waves, *J. Fluid Mech.*, *285*, 95–122, doi:10.1017/S0022112095000474.

Hughes, B. A., and J. F. R. Gower (1983), SAR imagery and surface truth comparisons of internal waves in Georgia Strait, British Columbia, Canada, *J. Geophys. Res.*, *88*(C3), 1809–1824, doi:10.1029/JC088iC03p01809.

Johnson, R. S. (1982), On the oblique interaction of a large and a small solitary wave, *J. Fluid Mech.*, *120*, 49–70.

LeBlond, P. H., and L. A. Mysak (1978), *Waves in the Ocean*, Elsevier, Amsterdam.

Liu, A. K., and M.-K. Hsu (1998), Nonlinear internal wave interaction in the China seas, in *The 1998 WHOI/IOS/ONR Internal Solitary Wave Workshop: Contributed Papers*, *Tech. Rep. WHOI-99-07*, pp. 140–142, Woods Hole Oceanogr. Inst., Woods Hole, Mass.

Lynett, P., and P. L.-F. Liu (1998), Numerical modeling of internal wave-wave interactions, in *The 1998 WHOI/IOS/ONR Internal Solitary Wave Workshop: Contributed Papers*, *Tech. Rep. WHOI-99-07*, pp. 218–223, Woods Hole Oceanogr. Inst., Woods Hole, Mass.

Matsuno, Y. (1998), Oblique interaction of interfacial solitary waves in a two-layer deep fluid, *Proc. R. Soc. London A*, *454*, 835–856.

Melville, W. K. (1980), On the Mach reflexion of a solitary wave, *J. Fluid Mech.*, *98*, 285–297.

Miles, J. W. (1977), Obliquely interacting solitary waves, *J. Fluid Mech.*, *79*, 157–169.

Oikawa, M. (1984), On the weak interactions of the Benjamin-Ono solitons, *Bull. Res. Inst. Appl. Mech. Kyushu Univ.*, *60*, 467–472.

Ono, H. (1975), Algebraic solitary waves in stratified fluids, *J. Phys. Soc. Jpn.*, *39*, 1082–1091.

Osborne A. R. (2010), *Nonlinear Ocean Waves and the Inverse Scattering Transform*, *Int. Geophys. Ser.*, vol. 97, 917 pp., Elsevier, Burlington, Mass.

Pawlowicz, R. (2003), Quantitative visualization of geophysical flows using low-cost oblique digital time-lapse imaging, *IEEE J. Oceanic Eng.*, *28*(4), 699–710, doi:10.1109/JOE.2003.819310.

Pawlowicz, R., O. Riche, and M. Halverson (2007), The circulation and residence time of the Strait of Georgia using a simple mixing-box approach, *Atmos. Ocean*, *45*(2), 173–193.

Shand, J. A. (1953), Internal waves in Georgia Strait, *Eos Trans. AGU*, *34*(6), 849.

Soomere, T. (2007), Nonlinear components of ship wake waves, *Appl. Mech. Rev.*, *60*(3), 120–138.

Soomere, T., and J. Engelbrecht (2006), Weakly two-dimensional interaction of solitons in shallow water, *Eur. J. Mech. B Fluids*, *25*, 636–648, doi:10.1016/j.euromechflu.2006.02.008.

Tanaka, M. (1993), Mach reflection of a large-amplitude solitary wave, *J. Fluid Mech.*, *248*, 637–661.

Tsuji, H., and M. Oikawa (2001), Oblique interaction of internal solitary waves in a two-layer fluid of infinite depth, *Fluid Dyn. Res.*, *29*, 251–267.

Turner, J. S. (1973), *Buoyancy Effects in Fluids*, Cambridge Univ. Press, Cambridge, U. K.

Wang, C. (2009), Geophysical observations of nonlinear internal solitary-like waves in the Strait of Georgia, PhD thesis, Univ. of B. C., Vancouver, B. C., Canada.

Wang, C., and R. Pawlowicz (2011), Propagation speeds of strongly nonlinear near-surface internal waves in the Strait of Georgia, *J. Geophys. Res.*, *116*, C10021, doi:10.1029/2010JC006776.

Whitham, G. B. (1974), *Linear and Nonlinear Waves*, John Wiley, New York.